Organic Electronics 34 (2016) 42–49

Contents lists available at ScienceDirect

Organic Electronics

journal homepage: www.elsevier.com/locate/orgel

Dramatically enhanced performances and ideally controlled nano-morphology via co-solvent processing in low bandgap polymer solar cells

Yu Jin Kim [a, 1], Woogsik Jang [b, 1], Sunyong Ahn [b], Chan Eon Park [a, *], Dong Hwan Wang [b, **]

[a] POSTECH Organic Electronics Laboratory, Department of Chemical Engineering, Pohang University of Science and Technology, Pohang, 790-784, Republic of Korea
[b] School of Integrative Engineering, Chung-Ang University, 84 Heukseok-Ro, Dongjak-gu, Seoul, 156-756, Republic of Korea

ARTICLE INFO

Article history:
Received 5 March 2016
Received in revised form
6 April 2016
Accepted 7 April 2016
Available online 14 April 2016

Keywords:
Bulk heterojunction solar cell
Polymer solar cell
Co-solvent
Nanoscale morphology
Phase separation

ABSTRACT

The device performance of photovoltaics with a polymer:fullerene bulk heterojunction (BHJ) structure, consisting of DT-PDPP2T-TT donor polymer and poly(3-hexylthiophene):[6,6]phenyl-C_{61}-butyric acid methyl ester ($PC_{61}BM$) acceptor compound, was investigated as a function of co-solvent composition. An enhancement of the photocurrent density and fill factor is observed in diodes made by spin-coating with chloroform mixed with *ortho*-dichlorobenzene, which allows a significantly higher device efficiency of 5.55% compared to diodes made from neat chloroform (efficiency = 3.61%). To clarify the role of the co-solvent, we investigated the nanoscale morphology with AFM, TEM and 2D-GIWAXS techniques and also the free-charge carrier mobility via space-charge limited current theory. We obtained the result that, under such supersaturated conditions, co-solvents induce increased polymer crystalline aggregation into a 3D phase structure and boost charge-carrier transport characteristics. This provides a rational basis for the development of ideally-controlled BHJ films that yield efficient DT-PDPP2T-TT:PCBM solar cells. Therefore, carefully selecting solvent mixtures provides an approach toward efficient low bandgap polymer solar cells.

1. Introduction

Polymer solar cells (PSCs) have attracted considerable interest in recent years, due to their potential for rapid energy payback time and low-cost fabrication of flexible plastic solar modules [1–3]. Bulk heterojunction PSCs, typically consisting of an active layer with a donor-acceptor blend film (electron-donating polymers, electron-accepting fullerenes), have garnered significant attention for reaching a high power conversion efficiency (PCE) of up to 9–10% [4,5]. The strategy for power conversion efficiency (PCE) improvement of BHJ PSCs could be summarized as the following: the design and synthesis of polymeric electron-donating materials [6–10]; the development of novel device architectures [11–13]; the control of nanoscale BHJ morphology [14,15]; and, selecting interfacial layers for better charge carrier collection [16].

Among the promising device configurations, controlling the degree of phase separation for the BHJ morphology is one of the best strategies for boosting the performance of PSCs. Therefore, several methods have been applied to modify or control the morphology of the BHJ blends such as solvent (vapor) annealing, thermal annealing, and selection of the processing solvent or mixed solvent [17–23].

For example, very recently, Janssen et al. reported the realization of desired polymer aggregation via a co-solvent in diketopyrrolopyrrole (DPP)-based solar cells [24,25]. In a similar period, Cheng et al. reported that using mixed chloroform:dichloromethane solvents rather than chloroform is better for the improvement of efficiency due to resultant ordered microstructural features of active layer materials [26]. Moreover, Jenekhe et al. studied all-polymer PSEHTT/PNDIS-HD films with which a co-solvent controlled phase-separated domain sizes [27]. According to these works, it can be concluded that crystallinity as well as domain size in the blends can be effectively tuned by using binary solvent mixtures. As a result, how to screen for a suitable solvent system with which to

* Corresponding author.
** Corresponding author.
E-mail addresses: cep@postech.ac.kr (C.E. Park), king0401@cau.ac.kr (D.H. Wang).
[1] Y. J. Kim and W. Jang contributed equally to this work.

http://dx.doi.org/10.1016/j.orgel.2016.04.010
1566-1199/

adjust the morphology of the active layer is one of the key issues in the quest for high performance PSCs.

Based on the aforementioned considerations, we introduced two functional solvents as processing solvents for low bandgap DT-PDPP2T-TT:PCBM solar cells, to create efficient bulk heterojunction PSC devices (device structure; Fig. 1a). Indeed, we recently reported a DT-PDPP2T-TT:PCBM system in tandem organic solar cells that exhibits superior photovoltaic properties with a PCE of 7.4% [28]. Although this copolymer shows excellent performances, the detailed understanding and information on the effects of the co-solvents are not in that study.

Therefore, for the present article on the DT-PDPP2T-TT:PCBM blend we systematically studied the effect of the co-solvent on device performance using two commonly-used mixed solvents: chloroform (CF) and *ortho*-dichlorobenzene (DCB). To clarify the role of the co-solvents, the morphological evolution of the blends was demonstrated by atomic force microscopy and grazing incidence wide angle X-ray scattering. Moreover, free-carrier transport characteristics were investigated using the space-charge limited current model.

2. Results and discussion

Before investigating for the effects of co-solvents on device performance, we have first rechecked the energy levels of each component's band structure, as shown in Fig. 1b. The difference between DT-PDPP2T-TT and $PC_{61}BM$ of the highest occupied molecular orbital (HOMO) energy was ca. 1.0 eV, which is sufficient to block the electrons diffused from the DT-PDPP2T-TT polymer [29]. Furthermore, considering the large lowest unoccupied molecular orbital (LUMO) offset (0.6 eV) between the two active materials in the solid-state films, the charge separation process from the excitons in the DT-PDPP2T-TT domain to the LUMO level of the $PC_{61}BM$ domain is expected to occur efficiently [29].

2.1. The effect of co-solvents on device efficiency

A series of polymer solar cells with DT-PDPP2T-TT:PCBM as the active layer were fabricated to investigate the effect of mixed solvents on photovoltaic performance. Fig. 2a exhibits the distinct differences in the current density-voltage (*J-V*) characteristics for layers processed using chloroform (CF) with and without 50, 100 and 200 vol% DCB as co-solvent (detailed device parameters are in Table 1). For the solar cell devices processed with neat CF as solvent, an optimized PCE of 3.61% was obtained with an open-circuit voltage (*Voc*) of 0.71 V, a short-circuit current (J_{SC}) of 8.28 mA cm^{-2} and a fill factor (FF) of 62%. By using CF:DCB (1:0.5, v/v) mixed solvents, an enhanced photovoltaic performance with a PCE of 4.76% was obtained. Furthermore, further increases in the J_{SC} (from 11.24 mA cm^{-2} to 11.79 mA cm^{-2}) and FF (from 62% to 65%) were obtained by using the co-solvent (CF:DCB = 1:1) and thus the PCE was increased to 5.55%. However, when the concentration of DCB was further increased (CF:DCB = 1:2), both J_{SC} and FF were decreased, (but not the *Voc* value)— below the values that were obtained by using CF only. As a result, the champion device was obtained when a CF:DCB solvent blend with the optimal composition of 1:1 was processed. We expected that by processing CF:DCB co-solvents, particularly with 1:1 vol ratios, the main impact would be the enhanced photocurrent and fill factor values. For these J_{SC} improvements to have occurred, we believe that the differences in the photovoltaic performances are mainly due to the differences in network morphology and molecular packing structures, as is discussed below.

In addition, to be able to investigate the impact on the fullerene compounds, the DT-PDPP2T-TT:$PC_{71}BM$ device spin-coated from CF:DCB 1:1 v/v was recorded; they show no significant effect on the $PC_{71}BM$ compound, which suggests that considerable variation of the device performances possibly due to processing solvents.

In order to further confirm the effect of the co-solvent on PSC performance, incident photon to current efficiency (IPCE) spectra were measured and are shown in Fig. 2b. The IPCE spectra of DT-PDPP2T-TT:$PC_{61}BM$ PSCs made with CF and with CF:DCB show that devices processed with CF:DCB as solvent have quite higher IPCE values in the entire wavelength range. Moreover, according to the IPCE curves, the calculated J_{SC} is 8.36 mA cm^{-2} for CF-devices, 12.19 mA cm^{-2} for CF:DCB-polymer:$PC_{61}BM$ devices, and 12.36 mA cm^{-2} for CF:DCB-polymer:$PC_{71}BM$ devices, which is in good agreement with the J_{SC} results obtained from *J-V* characteristics curves within a 3% error [30]. And also, with regard to fullerene derivatives ($PC_{61}BM$ and $PC_{71}BM$), the IPCE spectra show that the IPCE value of $PC_{71}BM$ is superior to that of $PC_{61}BM$ in the short-wavelength range (400 nm–700 nm), but inferior in the long-wavelength range (700 nm–900 nm). The effect of using fullerene derivatives is inadequate to enhance the PCE, and so controlling the co-solvent system for devices made of DT-PDPP2T-TT is more meaningful than changing the fullerene compounds.

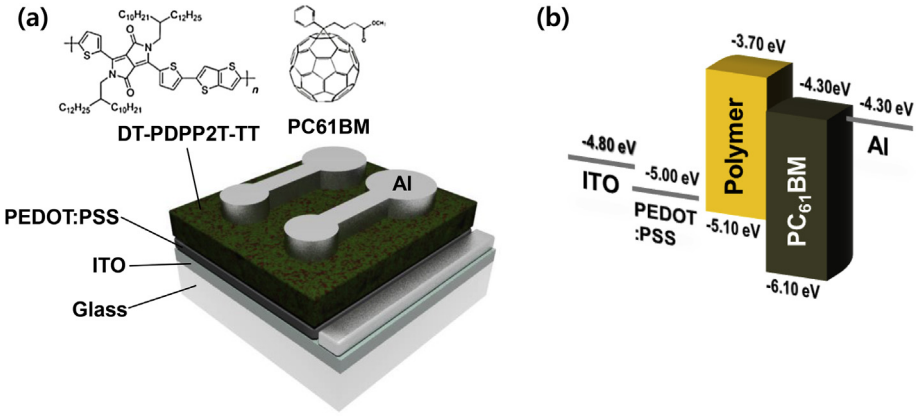

Fig. 1. (a) Conventional structure of ITO/PEDOT:PSS/DT-PDPP2T-TT:PCBM/Al and the molecular structures of the polymer and PCBM. (b) Schematic diagram for band energy levels of the proposed device structure.

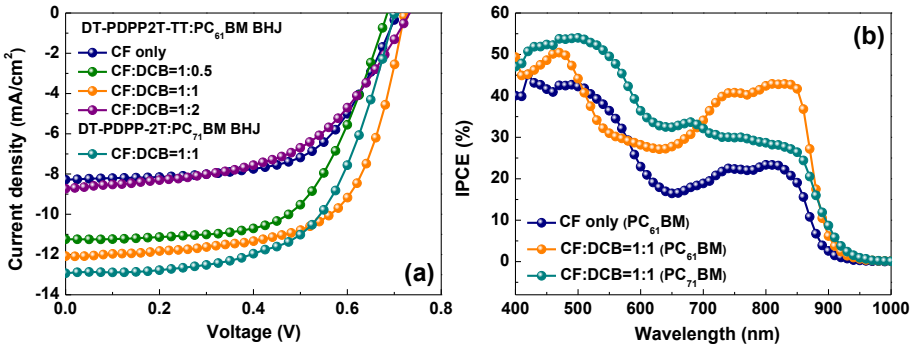

Fig. 2. (a) Current density (*J*)-voltage (*V*) curves of the DT-PDPP2T-TT:PCBM solar cells based on different solvent conditions and (b) IPCE spectra of DT-PDPP2T-TT:$PC_{61}BM$ and DT-PDPP2T-TT:$PC_{71}BM$ devices processed from different solvents.

Table 1
Photovoltaic results of DT-PDPP2T-TT:PCBM solar cells processed by different solvents.

DT-PDPP2T-TT:PCBM	V_{OC} [V]	J_{SC} [mA/cm^2]	FF [%]	PCE [%]	PCE [%][a]
CF only	0.71	8.28	62	3.61	3.61 ± 0.01
CF:DCB = 1:0.5	0.69	11.24	62	4.76	4.83 ± 0.16
CF:DCB = 1:1	0.72	11.79	65	5.55	5.50 ± 0.09
CF:DCB = 1:2	0.73	8.73	52	3.35	2.94 ± 0.41
CF:DCB = 1:1($PC_{71}BM$)	0.71	12.93	61	5.52	5.50 ± 0.03

[a] Average data from 10 devices.

2.2. Nanoscale morphology investigated by AFM, TEM and the 2D-GIWAXS technique

The significant differences in device performance with different solvent conditions may originate from different morphology structures, and the morphology characteristics of DT-PDPP2T-TT:$PC_{61}BM$ blends spin-coated from CF and 1:1 CF:DCB solvents were evaluated by atomic force microscopy (AFM), by transmission electron microscopy (TEM) and by two-dimensional grazing-incidence wide-angle X-ray scattering (2D-GIWAXS) (Fig. 3a–f).

For some polymer:fullerene combinations, it was shown that the effect of a co-solvent is to increase domain sizes, which is most commonly attributed to polymer aggregation in solution [31,32]. From the AFM height images (Fig. 3a–b), DT-PDPP2T-TT:$PC_{61}BM$ films processed with only CF solvent show a perforated surface with a considerable number of pores, which is not ideal for efficient exciton dissociation and charge carrier transport. In contrast, the DT-PDPP2T-TT:$PC_{61}BM$ films spin-coated from CF:DCB co-solvent exhibit ideally-aggregated and phase-separated surfaces with fine domain sizes (particularly without holes). These morphologies indicate that the pronounced formation of finely-packed domains originated from improvements in the intermolecular packing structure of the compounds, which allows efficient charge carrier movement [33]. Furthermore, these different morphological characteristics in only CF and CF:DCB-treated films are associated with the solvent's drying kinetics; because the DCB has relatively higher boiling point, when spin coating is processed with solution containing CF:DCB co-solvents, their allow sufficient time to be able to re-arrange for the active compounds with more ordered packing phases [34].

This morphology trend is also revealed in the TEM results (Fig. 3c–d). The areas of bright contrast are polymer rich (due to a lower electron density) and areas of dark contrast are rich in PCBM. The thin film of DT-PDPP2T-TT:$PC_{61}BM$ processed with CF:DCB exhibits distinctly enhanced phase separation with well-connected polymer and PCBM domains. These observations are consistent with the dramatic increase in J_{SC} values of the photovoltaic devices processed from binary mixture solvents [35]. Finally, these results demonstrate that the active (surface/bulk) morphology of DT-PDPP2T-TT:$PC_{61}BM$ blends was varied by using a co-solvent mixture (CF:DCB 1:1).

To improve upon the information on the active morphology for the blend layers, the crystalline nanostructure of the BHJ layers was investigated by employing a 2D-GIWAXS technique. Fig. 3e–f shows the 2D-GIWAXS scattering patterns and detailed interference profiles (Fig. 3g–h) along the out-of-plane and in-plane directions for CF and CF:DCB films. Both DT-PDPP2T-TT:$PC_{61}BM$ blends cast from CF and CF:DCB solutions exhibit resolved first-(100) and second-order (200) interlamellar reflection peaks along the out-of-plane direction ($q_z \approx 0.28$ Å^{-1}, d-spacing ≈ 23.27 Å). Moreover, the broad scattering peak at $q \approx 1.44$ Å^{-1} is characteristic, as having come from fullerene moieties [35]. Above all, the scattering peaks remain at the same positions but their intensities are quite different. We interpret this behavior as meaning that there is a relatively large increase in X-ray scattering intensity between the film cast from CF and the one cast from CF:DCB, indicating enhanced crystallinity and more oriented molecular packing [36]. Therefore, the 2D-GIWAXS data suggest that both the exciton diffusion and charge carrier transport are expected to benefit from the increased molecular packing with the CF:DCB co-solvent system, which probably explains the better device performance [36].

2.3. X-ray diffraction analysis

In the device performance section above, we argued that the DT-PDPP2T-TT:PCBM blends were more strongly influenced by the choice of the processing solvent than by the choice of fullerene compounds. To confirm this statement, X-ray diffraction (XRD) measurements on the polymer:$PC_{61}BM$ and polymer:$PC_{71}BM$ blend films were carried out to investigate the crystalline packing order, structural information and crystallite sizes (Fig. 4 and Table 2). Before investigating the XRD patterns of blend films, an XRD profile of neat DT-PDPP2T-TT films (Fig. 4a) was analyzed: the (*h*00) diffraction peak, with the scattering angle of (100) diffractions at $2\theta = 2.84°$, was observed along with up to third-order reflections which suggests a well-organized "edge-on" orientation [37]. In addition, a (010) reflection peak appears at $2\theta = 20.32°$, and thus it was determined that the corresponding π–π intermolecular stacking distance was 3.04 Å.

Upon adding $PC_{61}BM$ or $PC_{71}BM$ in DT-PDPP2T-TT systems (Fig. 4b-c), both XRD patterns showed a new isotropic broad reflection at $2\theta = 13.52°$ due to scattering from the PCBM domains [36]. Most of all, the intermolecular packing of the polymer crystalline domains intactly remained in both blend films, particularly

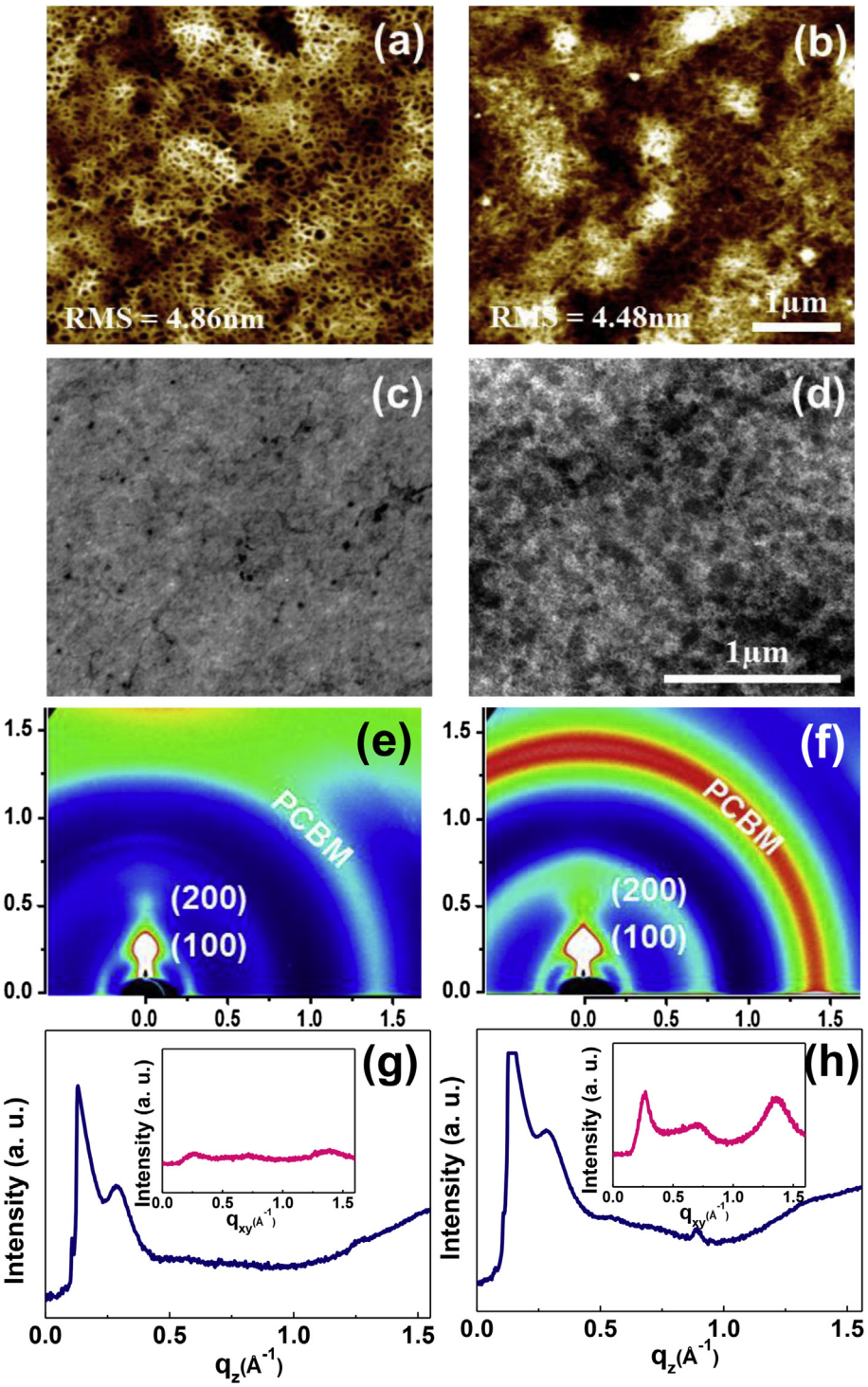

Fig. 3. Nanoscale morphology characteristics for DT-PDPP2T-TT:$PC_{61}BM$ films processed with CF (left column) and 1:1 CF:DCB solutions (right column): (a and b) AFM height images, (c and d) TEM images, (e and f) 2D-GIWAXS patterns and (g and h) line-cut intensity of the out-of-plane direction (the inset exhibits extraction profiles of the in-plane direction).

for the (100) scattering peak, and quite similar XRD diffractograms were revealed. So according to the XRD data, there is no variation of the bulk morphology of the PCBM compounds due to fullerene derivative choices.

To understand these results, we calculated crystallite sizes deduced from the full width at half maximum (FWHM) of inter-lamellar peaks (100), which indicates the mean size of the polymer crystalline domains (Fig. 4d). The mean size of the ordered domains (τ) was determined using Scherrer's formular, which is shown in following equation [38].

$$\tau = \frac{K\lambda}{\beta\,(FWHM)cos\theta}$$

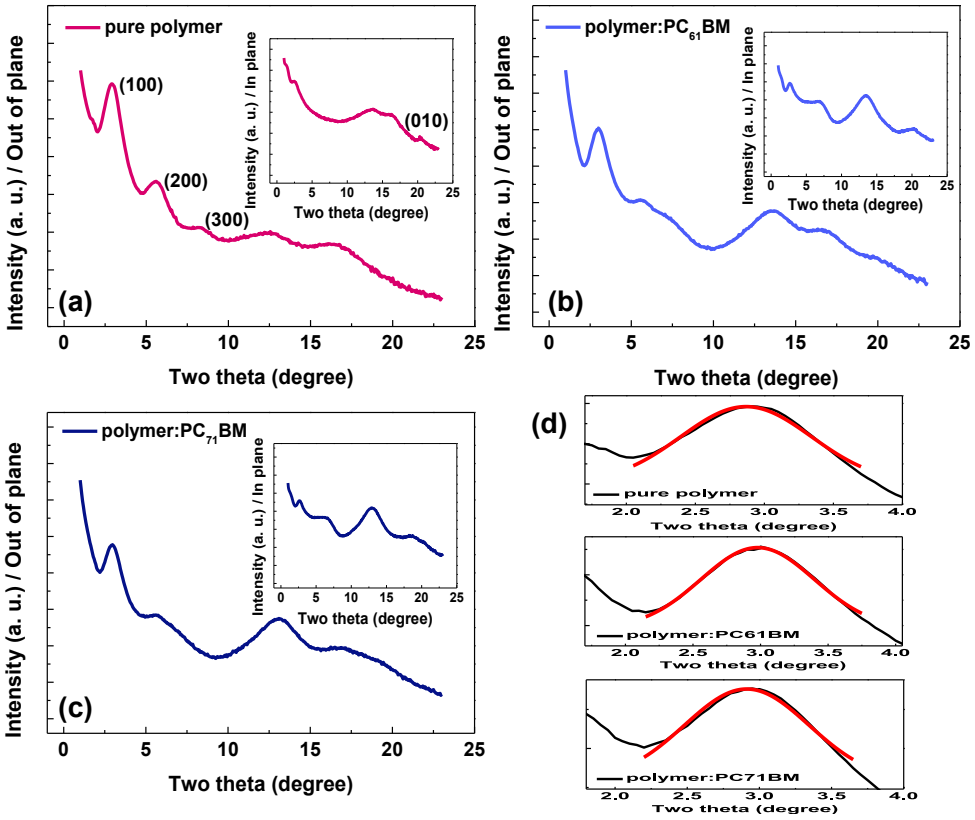

Fig. 4. Out-of-plane patterns of X-ray diffraction for (a) DT-PDPP2T-TT (b) DT-PDPP2T-TT:$PC_{61}BM$ (c) DT-PDPP2T-TT:$PC_{71}BM$ films (the insets respectively show in-plane XRD patterns of the pure polymer, polymer:$PC_{61}BM$ and polymer:$PC_{71}BM$ film). (d) Three fitting profiles in the (100) out-of-plane peak position were extracted using a Gaussian model.

Table 2
Peak list details of XRD patterns of pure polymer, polymer:$PC_{61}BM$ and polymer:$PC_{71}BM$ samples.

Active film	Peak (100) plane (°)	FWHM[a] (°)	Crystallite size (nm)
Pure_ DT-PDPP2T-TT	2.84	0.77	7.91
DT-PDPP2T-TT:$PC_{61}BM$	2.87	0.74	7.46
DT-PDPP2T-TT:$PC_{71}BM$	2.86	0.69	8.06

[a] Full width at half maximum.

where λ is the X-ray wavelength, β is the value of the FWHM of the (100) reflection peak, and θ is the Bragg angle. The calculated τ of DT-PDPP2T-TT crystallites showed significantly similar values for all films (7.91 nm for pure polymer films, 7.46 nm for polymer:$PC_{61}BM$ films and 8.06 nm for polymer:$PC_{71}BM$ films). This indicates that the nature of the PCBM does not affect the DT-PDPP2T-TT crystallinity characteristics. Therefore, we can conclude that the considerable differences in device performance are associated with distinct changes in nanoscale morphology due to different solvent processing.

2.4. Effect of co-solvents on charge carrier mobility

The relationships between charge carrier transport, and crystalline ordering and photovoltaic performance are established in prominent polymer systems. Therefore, to gain insight into the effect of co-solvents within polymer:PCBM bulk heterojunction blends on charge transport, space-charge limited current (SCLC) was used to map out the charge carrier mobilities in CF- and CF:DCB (1:1 v/v) treated films by measuring the *J-V* characteristics of single carrier devices in dark conditions and analyzing the results, as shown in Fig. 5a–b. The carrier mobility was extracted by fitting the *J-V* curves in the near quadratic region according to the modified Mott-Gurney equation [39]. Charge carrier mobilities of DT-PDPP2T-TT:$PC_{61}BM$ blend films deposited from CF were found to be 5.66×10^{-5} cm^2/V (hole) and 1.12×10^{-5} cm^2/V (electron), whereas DT-PDPP2T-TT:$PC_{61}BM$ blends processed from CF:DCB co-solvent had hole mobilities of 4.37×10^{-4} cm^2/V and electron mobilities of 2.46×10^{-4} cm^2/V, one order of magnitude higher. This is in good agreement with our expectation from the crystalline ordering analyses. Therefore, these higher carrier mobilities in the DT-PDPP2T-TT:$PC_{61}BM$ films processed using the CF:DCB co-solvent can explain the improved photovoltaic performance as due to enhanced J_{SC}, and thus the higher PCE values of these solar cell devices [40]. Also, slightly more balanced hole and electron transport appears in the blend film processed from CF:DCB co-solvent ($\mu_h/\mu_e = 1.77$, μ_h/μ_e of only CF-treated films is 5.05), which support the reason of relatively higher FF values in solar cells treated with CF:DCB co-solvent [41].

The results of charge carrier mobility as well as AFM, TEM and 2D-GIWAXS analyses allow the scenario presented in Fig. 5c to be drafted. The drawing should be understood as an illustration of the assumed significant changes of the microstructure morphology upon the introduction of the co-solvent, CF:DCB. In Fig. 5c, the green box and yellow ball show DT-PDPP2T-TT polymer and

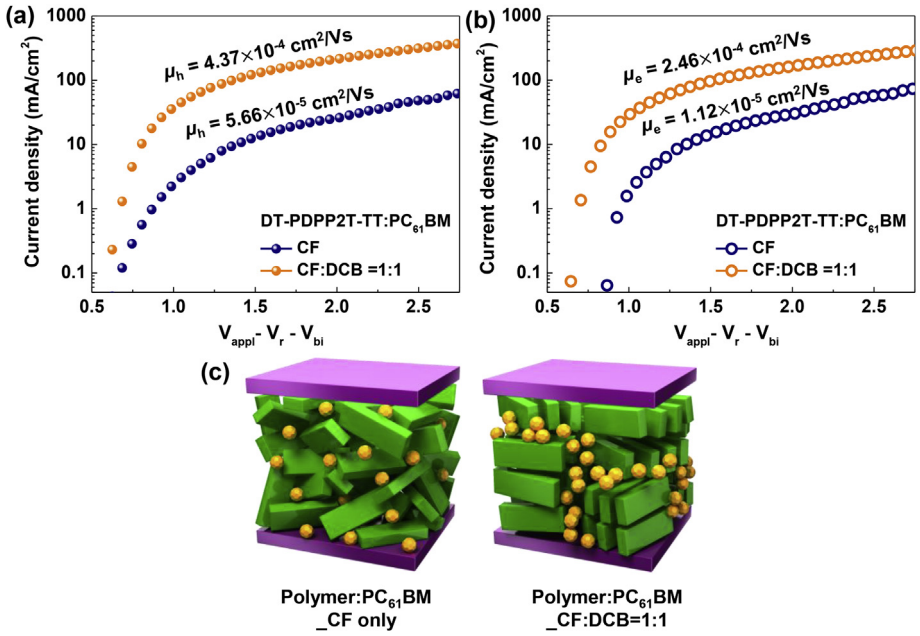

Fig. 5. The dark *J-V* characteristics of hole-only devices (a) and electron-only devices (b) for DT-PDPP2T-TT:$PC_{61}BM$ prepared by CF and CF:DCB (1:1, v/v). (c) A schematic illustration of the DT-PDPP2T-TT:$PC_{61}BM$ active layers processed with CF (left) and CF:DCB (1:1, v/v) (right).

$PC_{61}BM$, respectively. CF-treated polymer:$PC_{61}BM$ blends exhibit relatively randomly-stacked polymer and PCBM structure, whereas more ordered polymer packing structures and aggregated PCBM domains are shown in CF:DCB blends. Therefore, CF:DCB binary mixed solvents lead to more orientated polymer crystallinity and to a more three-dimensional phase structure in BHJ films than that do neat CF treatments, and thus indeed these ideally phase-aggregated polymer structures yield highly efficient low bandgap polymer solar cells.

3. Conclusions

In conclusion, by incorporating two functional solvents as the processing solvent, we are able to create efficient BHJ PSC devices with DT-PDPP2T-TT:PCBM as the active layer. The performance of these diodes shows that mixing solvents (CF:DCB = 1:1, v/v) has a significant positive effect on the photocurrent density and fill factor values, and thus quite high 5.55% efficiency is obtained improved ca. 54% over a device processed with neat CF (PCE = 3.61%). These enhanced performances of PSCs should strongly depend on the nanoscale morphology of active layers, on increased crystallinity of packing structures induced by the co-solvent. AFM, TEM and 2D-GIWAXS analyses support this conclusion, and also charge carrier measurements point out that one order of magnitude higher mobility is found in the devices treated with binary mixed solvents. As a result, these findings suggest that the choice of mixed solvent provides an effective method with which to exquisitely fine-tune and optimize the morphology of narrow bandgap conjugated polymer-fullerene compositions, for highly efficient, high-performance PSCs.

4. Experimental

4.1. Materials

DT-PDPP2T-TT polymer (M_n = 780 K and PDI = 3.25) was purchased from Solarmer Material Inc and PCBM ($PC_{61}BM$ and $PC_{71}BM$) was obtained from Nano-C Inc.

4.2. General measurements

Non-contact mode AFM was performed using a Park NX10 to obtain the surface morphology for DT-PDPP2T-TT:$PC_{71}BM$ blends processed with CF or CF:DCB solvents. TEM images were obtained using a HITACHI-7600 operated at 100 kV. The active layers were floated from the PEDOT:PSS (water-soluble)-coated substrates onto the surface of dematerialized water and picked up with 200-mesh copper grids. 2D-GIWAXS specular scans were obtained by using the 3C beam lines and XRD measurements were performed using the 5A beam lines at the Pohang Accelerator Laboratory. The 2D-GIWAXS measurements were carried out with a sample-to-detector distance of 210.541 mm. The data were typically collected for 30 s by using an X-ray radiation source at λ = 1.1189 nm with a 2D charge-coupled detector (CCD) (Roper Scientific, Trenton, NJ, USA). The samples were mounted on a lab-built z-axis goniometer equipped with a vacuum chamber. The incidence angle a_i of the X-ray beam was set at 0.12°, which is an intermediate value between the critical angles of the films and the substrate ($a_{c,f}$ and $a_{c,s}$). XRD experiments were performed with a wavelength 1.071 Å. For the 2D-GIWAXS and XRD measurement, the samples were prepared as follows: an active layer (DT-PDPP2T-TT or DT-PDPP2T-TT:PCBM) was spin-coated on a Si substrate, the same as in the actual photovoltaic devices.

4.3. Solar cell fabrication and characterization

The polymer solar cells were fabricated using a solution process with a conventional structure of glass/ITO/PEDOT:PSS/active layer (DT-PDPP2T-TT:PCBM)/Al. The glass/ITO substrates were first cleaned by ultrasonic treatment in detergent, deionized water, acetone and isopropyl alcohol under ultrasonication for 20 min each, and subsequently dried with blowing nitrogen. Prior to the fabrication of the organic layers, the glass/ITO substrates were treated with UV-ozone for 20 min. A PEDOT:PSS thin layer (ca. 40 nm) (Clevios P VP AI 4083, filtered at PVDF 0.45 μm) was spin-coated at 4000 rpm for 60 s onto the ITO surface. And then, the active layer of DT-PDPP2T-TT:PCBM was spin-coated onto the

PEDOT:PSS layer in a glove box (the solution of DT-PDPP2T-TT:PCBM (1:3 w/w) is made with a concentration of 12 mg/ml in CF or CF:DCB (ratios of 1:0.5, 1:1 and 1:2)) (The thickness of the active layer processed with CF and CF:DCB is 258 nm and 253 nm, respectively). Afterward, 100 nm Al was deposited sequentially under high vaccum (4.0×10^{-6} Torr) by thermal evaporation. The effective area of each cell was around 0.15 cm^2. The photocurrent–voltage (*J-V*) curve of the solar cell device was obtained using a Keithley 2400 Source Measure Unit instrument and determined under the illumination of simulated 100 mW/cm^2 Air Mass 1.5 Global (AM 1.5 G) (ZIVE SP1). Incident photon-to-current efficiency (IPCE) spectra were obtained using PV measurements.

4.4. Hole mobility measurements

Space-charge limited currents have been tested in hole- and electron-only devices with a configuration of ITO/PEDOT:PSS/DT-PDPP2T-TT:PC_{61}BM/Au and Al/DT-PDPP2T-TT:PC_{61}BM/Al, respectively. The devices were prepared following the same procedure described in the experimental section for solar cell devices, except for the metal electrode. The carrier mobilities were extracted by fitting the dark current to the model of a Mott-Gurney relation, which is described as

$$J = \frac{9}{8}\varepsilon_0\varepsilon_r\mu_{h/e}\frac{V^2}{L^3}\exp\left(\frac{0.89\beta}{\sqrt{L}}\sqrt{V}\right)$$

where J represents the current density, L is the thickness of the active layer, $\mu_{h/e}$ is hole/electron carrier mobility, ε_0 and ε_r are respectively the electric permittivity of free space and the relative dielectric constant of the active layer, β is the electric field-activation factor. $V = V_{appl} - V_r - V_{bi}$, where V_{appl} is the applied voltage, V_r represents the voltage drop due to contact resistance and series resistance across the electrodes, and V_{bi} is the built-in voltage.

Acknowledgements

This research was supported by the Basic Science Research Program, through the National Research Foundation of Korea (NRF), funded by the Ministry of Science, ICT & Future Planning (2014R1A1A1002419). This study was also supported by a grant (2011-0031639) from the Center for Advanced Soft Electronics under the Global Frontier Research Program of the Ministry of Education, Science and Technology.

References

[1] A.J. Heeger, Bulk heterojunction solar cells: understanding the mechanism of operation, Adv. Mater. 26 (2014) 10–28.
[2] Y. Liu, J. Zhao, Z. Li, C. Mu, W. Ma, H. Hu, K. Jiang, H. Lin, H. Ade, H. Yan, Aggregation and morphology control enables multiple cases of high-efficiency polymer solar cells, Nat. Commun. 5 (2014) 5293.
[3] G. Li, R. Zhu, Y. Yang, Polymer solar cells, Nat. Photonics 6 (2012) 153–161.
[4] L. Huo, T. Liu, X. Sun, Y. Cai, A.J. Heeger, Y. Sun, Single-junction organic solar cells based on a novel wide-bandgap polymer with efficiency of 9.7%, Adv. Mater. 27 (2015) 2938–2944.
[5] C.–C. Chen, W.–H. Chang, K. Yoshimura, K. Ohya, J. You, J. Gao, Z. Hong, Y. Yang, An efficient triple-junction polymer solar cell having a power conversion efficiency exceeding 11%, Adv. Mater. 26 (2014) 5670–5677.
[6] C. Duan, A. Furlan, J.J. van Franeker, R.E.M. Willems, M.M. Wienk, R.A.J. Janssen, Wide-bandgap benzodithiophene-benzothiadiazole copolymers for highly efficient multijunction polymer solar cells, Adv. Mater. 27 (2015) 4461–4468.
[7] Z. Zhang, F. Lin, H.–C. Chen, H.–C. Wu, C.–L. Chung, C. Lu, S.–H. Tung, W.–C. Chen, K.–T. Wong, P.–T. Chou, A silole copolymer containing a ladder-type heptacylic arene and naphthobisozadizole moieties for highly efficient polymer solar cells, Energy Environ. Sci. 8 (2015) 552–557.
[8] H.–C. Chen, Y.–H. Chen, C.-C. Liu, Y.–C. Chien, S.–W. Chou, P.–T. Chou, Prominent short-circuit currents of fluorinated quinoxaline-based copolymer solar cells with a power conversion efficiency of 8.0%, Chem. Mater. 24 (2012) 4766–4772.
[9] Z. Shi, I.W.H. Ka, X. Wang, C. Vijila, F. Wang, G. Li, W.W. Tjiu, J. Li, J. Xu, Low band-gap weak donor-strong acceptor conjugated polymer for organic solar cell, RSC Adv. 5 (2015) 98876–98879.
[10] Q.–C. Yu, W.–F. Fu, J.–H. Wan, X.–F. Wu, M.–M. Shi, H.–Z. Chen, Evaluation of heterocycle-modified pentathiophene-based molecular donor materials for solar cells, ACS Appl. Mater. Interfaces 6 (2014) 5798–5809.
[11] S.H. Park, I. Shin, K.H. Kim, R. Street, A. Roy, A.J. Heeger, Tandem solar cells made from amorphous silicon and polymer bulk heterojunction sub-cells, Adv. Mater. 27 (2014) 298–302.
[12] M. Zhang, F. Zhang, Q. An, Q. Sun, W. Wang, J. Zhang, W. Tang, Highly efficient ternary polymer solar cells by optimizing photon harvesting and charge carrier transport, Nano Energy 22 (2016) 241–254.
[13] Q. An, F. Zhang, J. Zhang, W. Tang, Z. Deng, B. Hu, Versatile ternary organic solar cells: a critical review, Energy Environ. Sci. 9 (2016) 281–322.
[14] A. Zusan, B. Gieseking, M. Zerson, V. Dyakonov, R. Magerle, C. Deibel, The effect of diiodooctane on the charge carrier generation in organic solar cells based on the copolymer PBDTTT-C, Sci. Rep. 5 (2015) 8286.
[15] W. Huang, E. Gann, L. Thomsen, C. Dong, Y.–B. Cheng, C.R. McNeill, Unraveling the morphology of high efficiency polymer solar cells based on the donor polymer PBDTTT-EFT, Adv. Energy Mater. 5 (2015) 1401259.
[16] X. Ouyang, R. Peng, L. Ai, X. Zhang, Z. Ge, Efficient polymer solar cells employing a non-conjugated small-molecule electrolyte, Nat. Photonics 6 (2015) 520–525.
[17] G.L. Schulz, M. Lobert, I. Ata, M. Urdanilleta, M. Linden, A. Mishra, P. Bauerle, Functional tuning of A-D-A oligothiophenes: the effect of solvent vapor annealing on blend morphology and solar cell performance, J. Mater. Chem. A 3 (2015) 13738–13748.
[18] N.M. Murari, M.J. Crane, T. Earmme, Y.–J. Hwang, S.A. Jenekhe, Annealing temperature dependence of the efficiency and vertical phase segregation of polymer/polymer bulk heterojunction photovoltaic cells, Appl. Phys. Lett. 104 (2014) 223906.
[19] A.K.K. Kyaw, D.H. Wang, C. Luo, Y. Cao, T.–Q. Nguyen, G.C. Bazan, A.J. Heeger, Effects of solvent additives on morphology, charge generation, transport, and recombination in solution-processed small-molecule solar cells, Adv. Energy Mater. 4 (2014) 1301469.
[20] J.J. van Franeker, S. Kouijzer, X. Lou, M. Turbiez, M.M. Wienk, R.A.J. Janssen, Depositing fullerenes in swollen polymer layers via sequential processing of organic solar cells, Adv. Energy Mater. 5 (2015) 1500464.
[21] C. Lu, H.–C. Chen, W.–T. Chuang, Y.–H. Hsu, W.–C. Chen, P.–T. Chou, Interplay of molecular orientation, film formation, and optoelectronic properties on isoindito- and thienoisoindigo-based copolymers for organic field effect transistor and organic photovoltaic applications, Chem. Mater. 27 (2015) 6837.
[22] J. Wang, F. Zhang, M. Zhang, W. Wang, Q. An, L. Li, Q. Sun, W. Tang, J. Zhang, Optimization of charge carrier transport balance for performance improvement of PDPP3T-based polymer solar cells prepared using a hot solution, Phys. Chem. Chem. Phys. 17 (2015) 9835–9840.
[23] J. Wang, F. Zhang, Q. An, M. Zhang, J. Zhang, W. Tang, Adjusting acceptor redistribution for highly efficient solvent additive-free polymer solar cells, J. Mater. Chem. C (2016), http://dx.doi.org/10.1039/C6TC00911E.
[24] J.J. van Franeker, M. Turbiez, W. Li, M.M. Wienk, R.A.J. Janssen, A real-time study of the benefits of co-solvents in polymer solar cell processing, Nat. Commun. 6 (2015) 6229.
[25] W. Li, K.H. Hendriks, W.S.C. Roelofs, Y. Kim, M.M. Wienk, R.A.J. Janssen, Efficient small bandgap polymer solar cells with high fill factors for 300 nm thick films, Adv. Mater. 25 (2013) 3182–3186.
[26] F.–C. Wu, Y.–H. Li, C.–J. Tsou, K.–C. Tung, C.–T. Yen, F.–S. Chou, F.-C. Tang, W.–Y. Chou, J. Ruan, H.–L. Cheng, Synergistic effects of binary-solvent annealing for efficient polymer-fullerene bulk heterojunction solar cells, ACS Appl. Mater. Interfaces 7 (2015) 18967–18976.
[27] T. Earmme, Y.–J. Hwang, S. Subramaniyan, S.A. Jenekhe, All-polymer bulk heterojunction solar cells with 4.8% efficiency achieved by solution processing from a co-solvent, Adv. Mater. 26 (2014) 6080–6085.
[28] D.H. Wang, A.K.K. Kyaw, J.H. Park, Enhanced fill factor of tandem organic solar cells incorporating a diketopyrrolopyrrole-based low-bandgap polymer and optimized interlayer, ChemSusChem 8 (2015) 331–336.
[29] K.A. Mazzio, C.K. Luscombe, The future of organic photovoltaics, Chem. Soc. Rev. 44 (2015) 78–90.
[30] A. Katsouras, N. Gasparini, C. Koulogiannis, M. Spanos, T. Ameri, C.J. Brabec, C.L. Chochos, A. Avgeropoulos, A systematic analysis of polymer molecular weight influence on the organic photovoltaic performance, Macromol. Rapid Commun. 36 (2015) 1778–1797.
[31] L. Ye, S. Zhang, W. Ma, B. Fan, X. Guo, Y. Huang, H. Ade, J. Hou, From binary to ternary solvent: morphology fine-tuning of d/a blends in pdpp3t-based polymer solar cells, Adv. Mater. 24 (2012) 6335–6341.
[32] P. Cheng, L. Ye, X. Zhao, J. Hou, Y. Li, X. Zhan, Binary additives synergistically the efficiency of all-polymer solar cells up to 3.45%, Energy Environ. Sci. 7 (2014) 1351–1356.
[33] Y. Huang, E.J. Kramer, A.J. Heeger, G.C. Bazan, Bulk heterojunction solar cells: morphology and Performance relationships, Chem. Rev. 114 (2014) 7006–7043.
[34] K.A. Mazzio, C.K. Luscombe, The future of organic photovoltaics, Chem. Soc. Rev. 44 (2015) 78–90.

[35] P. Müller-Buschbaum, The active layer morphology of organic solar cells probed with grazing incidence scattering techniques, Adv. Mater. 26 (2014) 7692–7709.
[36] J. Min, Y.N. Luponosov, N. Gasparini, M. Richter, A.V. Bakirov, M.A. Shcherbina, S.N. Chvalun, L. Grodd, S. Grigorian, T. Ameri, S.A. Ponomarenko, C.J. Brabec, Effects of alkyl terminal chains on morphology, charge generation, transport, and recombination mechanisms in solution-processed small molecule bulk heterojunction solar cells, Adv. Energy Mater. 5 (2015) 1500386.
[37] S. Mukherjee, C.M. Proctor, G.C. Bazan, T. –Q. Nguyen, H. Ade, Significance of average domain purity and mixed domains on the photovoltaic performance of high-efficiency solution-processed small-molecule bhj solar cells, Adv. Energy Mater. 5 (2015) 1500877.
[38] Y. Yang, W. Chen, L. Dou, W.–H. Chang, H.–S. Duan, B. Bob, G. Li, Y. Yang, High-performance multiple-donor bulk heterojunction solar cells, Nat. Photonics 9 (2015) 190–198.
[39] H.T. Nicolai, G.A.H. Wetzelaer, M. Kuik, A.J. Kronemeijer, B. Boer, P.W.M. Blom, Space-charge-limited hole current in poly(9,9-dioctylfulorene) diodes, Appl. Phys. Lett. 96 (2010) 172107.
[40] B. Bouthinon, R. Clerc, J. Vaillant, J.–M. Verilhac, J. Faure-Vincent, D. Djurado, I. Ionica, G. Man, A. Gras, G. Pananakakis, R. Gwoziecki, A. Kahn, Impact of blend morphology on interface state recombination in bulk heterojunction organic solar cells, Adv. Funct. Mater. 25 (2015) 1090–1101.
[41] Y. Kim, S. Ahn, D.H. Wang, C.E. Park, A mechanistic understanding of a binary additive system to synergistically boost efficiency in all-polymer solar cells, Sci. Rep. 5 (2015) 18024.